Applied Radiation and Isotopes 229 (2026) 112377

Contents lists available at ScienceDirect

Applied Radiation and Isotopes

journal homepage: www.elsevier.com/locate/apradiso

Experimental cross sections and production feasibility of ^{61}Cu via ^{59}Co(α, 2n) for PET imaging using medium-energy alpha beams

Irene Cardani [a,1], Michele Colucci [a,1,*], Etienne Nigron [b], Arnaud Guertin [c], Mariagabriella Marrella [a,d], Ferid Haddad [b,c], Flavia Groppi [a], Simone Manenti [a,*]

[a] LASA Laboratory, Department of Physics of the University of Milan and INFN-MI, Via Fratelli Cervi, 201, Segrate, 20054, Italy
[b] GIP Arronax, 1, rue Aronnax, Saint-Herblain, 44817, France
[c] Laboratoire Subatech, CNRS/IN2P3, IMT Atlantique, Nantes Université, 4, rue Alfred Kastler, Nantes, 44307, France
[d] Department of Physics, University of Calabria, Via P. Bucci - Cubo 31C, Arcavacata di Rende, 87036, Italy

ARTICLE INFO

Keywords:
Radionuclide production
Alpha particle irradiation
PET imaging
Thick target yield
Medical cyclotron

ABSTRACT

The radionuclide ^{61}Cu is a promising positron emitter for PET imaging. We investigated its production via the ^{59}Co(α, 2n)^{61}Cu reaction in the energy range 14–59 MeV using the stacked-foil technique. Excitation functions for ^{61}Cu and co-produced radionuclides (^{60}Cu, $^{56–58,60,61}$Co, ^{59}Fe, ^{54}Mn) were measured by HPGe γ-spectrometry and compared with TALYS 1.96 predictions and previous datasets. Thick Target Yields (TTY) and radionuclidic purity (RNP) were calculated for different irradiation conditions. Results show that high-yield and high-purity ^{61}Cu production is achievable at 45 MeV on a 226 μm thick Co target (TTY^{EOB} ≈ 840 MBq μA^{-1}, RNP >99.9% after 3 h irradiation and 3.4 h waiting time) and feasible with emerging 30 MeV α-accelerators using a 76 μm thick Co target (TTY^{EOB} ≈ 420 MBq μA^{-1}, RNP > 99.9% after 3 h irradiation and 1.8 h waiting time). These findings support cost-effective production using inexpensive cobalt targets, reducing reliance on enriched materials. Practical implications for routine supply and synergy with α-accelerators designed for ^{211}At are discussed.

1. Introduction

Since the discovery of radioactivity, ionizing radiation has become crucial in medicine. Nuclear medicine utilizes trace amounts of radionuclides for diagnostics and radiotherapy. Radiopharmaceuticals, which combine a radioactive tracer with a drug, allow the targeted imaging and treatment of specific organs. Radionuclides that emit gamma photons are widely employed in Single Photon Emission Computed Tomography (SPECT), whereas positron-emitting radionuclides (β^+ emitters) are used in Positron Emission Tomography (PET) (Bashir et al., 2019). In radiotherapy, radionuclides emitting charged particles, such as alpha or beta particles are used to destroy diseased tissues (Coura-Filho et al., 2022). The concept of theranostic agents, which combine diagnostics and therapy, emerged to personalize treatments (Coura-Filho et al., 2022; Keinnen et al., 2019). Matched pairs of radionuclides, such as ^{44}Sc/^{47}Sc (Müller et al., 2018) and ^{124}I/^{131}I (Qaim, 2020), allow for both imaging and therapeutic applications in nuclear medicine.

In this area, an important element that presents several radioisotopes suitable for diagnosis, therapy, and theranostics is copper. There are five copper isotopes suitable for nuclear medicine due to their nuclear characteristics: ^{67}Cu, ^{64}Cu, ^{62}Cu, ^{61}Cu and ^{60}Cu.

^{67}Cu ($T_{1/2}$ = 61.83 h (IAEA-NDS, 2025)) is ideal for both SPECT imaging and therapy (Mou et al., 2022), but production is limited by the lack of producing facilities (Boschi et al., 2018). ^{64}Cu ($T_{1/2}$ = 12.7006 h (IAEA-NDS, 2025)), emitting both β^+ and β^- particles, is the most versatile for theranostics, although its production is challenging due to the need for highly enriched ^{64}Ni (Boschi et al., 2018). ^{62}Cu ($T_{1/2}$ = 9.67 min (IAEA-NDS, 2025)), with its short half-life, is used for dynamic organ studies, but the short lifespan of its generator limits its use (Boschi et al., 2018). ^{60}Cu ($T_{1/2}$ = 23.7 min (IAEA-NDS, 2025)), with a short half-life and presence of high energy gamma emissions, is less favored for clinical imaging due to poor image quality (Boschi et al., 2018).

This paper, instead, deals with the production of ^{61}Cu ($T_{1/2}$ = 3.339 h (IAEA-NDS, 2025)), useful for PET imaging due to its β^+ decay, although optimal spatial resolution is challenging due to high energy beta emission (Boschi et al., 2018). Several nuclear reactions have been explored to produce ^{61}Cu (Qaim, 2020; Hermanne et al., 2023), including bombarding natural or enriched zinc (Abbas et al., 2006) and nickel

* Corresponding authors.
E-mail addresses: michele.colucci@unimi.it (M. Colucci), simone.manenti@unimi.it (S. Manenti).
[1] These authors contributed equally to this work and share first authorship.

https://doi.org/10.1016/j.apradiso.2025.112377
Received 14 October 2025; Received in revised form 10 December 2025; Accepted 11 December 2025
Available online 15 December 2025

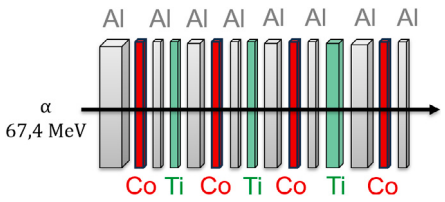

Fig. 1. Schematic representation of the stack-foil arrangement used in this work. The example refers to Stack 1 and illustrates the sequence of target foils, monitor foils, and catchers. The thickness is not representative of the real thickness of the foils.

targets with protons (Szelecsényi et al., 2006), though high target costs and material recovery issues are significant drawbacks (Szelecsényi et al., 2002). An alternative method is the ^{59}Co(α,2n) reaction, which could simplify radiochemical separation and reduce costs, as cobalt is monoisotopic and does not require expensive enriched targets like zinc or nickel.

Nowadays, there is growing interest in the construction of new α-particle accelerators with energies of around 30 MeV, aimed at producing radionuclides below this energy range, particularly for the production of ^{211}At, a promising alpha emitter for targeted alpha therapy (Qaim, 2024). In this context, evaluating the production of ^{61}Cu at energies equal to or lower than 30 MeV is of great interest for the advancement of the state-of-the-art production of radionuclides using such accelerator technology.

In this study, the excitation function of the ^{59}Co(α,2n)^{61}Cu nuclear reaction was investigated, along with those of the main copper contaminant (^{60}Cu) and other radionuclides produced in the process. The obtained cross section data are compared to previous experimental results from studies. This new dataset expands nuclear libraries and is used to determine the Thick Target Yields (TTY) and the RadioNuclidic Purity (RNP), exploring the potential for ^{61}Cu production using 30 MeV α-accelerators by assessing the feasibility of this production method.

Some of the studied reactions already have the potential to be used as monitor reactions to enrich the list of available monitor cross sections for alpha beams (Hermanne et al., 2018; Tárkányi et al., 2024). This possibility is further discussed in this work.

2. Materials and methods

To measure the excitation functions, 16 thin cobalt targets were irradiated with alpha particles using the stacked-foils method. Four separate stacks, each containing 4 cobalt foils, were arranged to cover the alpha particle energy range from 14 to 58.7 MeV. Within each stack, a 10 or 16 μm aluminum catcher foil was placed after every cobalt foil, which doubles as a monitor foil unless positioned next to another aluminum foil. Other aluminum foils, from 16 μm and 100 μm in thickness, were used as energy degraders and titanium foils of 10 and 20 μm of thickness were added to the stacks to serve as monitor foils in the last two stacks, where the energy was below 40 MeV. Aluminum foils 10 or 16 μm thick were used as catcher after titanium foils. An example of stack is reported in Fig. 1. All foils were purchased from GoodFellow Corporation (Huntingdon, UK) with different purities: Co foils have a purity of 99.6%, while Ti and Al foils have a purity of 99.9%. For each of them, the mass-thickness was determined by measuring the mass and the area with a highly accurate weigthing scale and caliper, with sensibilities up to 10^{-5} g and 10^{-5} m, respectively. The uncertainty on the mass thickness is set to 2% to account for stochastic and systematic errors in the measurements. All mass thicknesses are shown in Table 1. Then squares were cut with 2.5 × 2.5 cm^2 dimensions in order to be placed in a metal sample holder for the irradiation.

Table 1
Mass thickness calculated for each target. Nominal thickness are given by GoodFellow Corporation (Huntingdon, UK) where all foils were purchased. Uncertainty for the mass thickness (ρdx) is set to 2%.

Target	Nominal thickness (μm)	ρdx (mg m^{-2})
Cobalt	2.5	2.30
	7	5.84
Aluminum	10	2.80
	25	6.54
	50	13.2
	114	32.9
	250	68.0
	1000	271
Titanium	10	4.35
	20	8.14

Table 2
Average energy of the beam in each cobalt foils of the four irradiated stacks with associated uncertainty.

Stack	E_1 (MeV)	E_2 (MeV)	E_3 (MeV)	E_4 (MeV)
1st	58.7 ± 1.0	56.2 ± 1.1	53.6 ± 1.2	48.2 ± 1.5
2nd	50.8 ± 1.4	45.5 ± 1.7	43.2 ± 1.8	39 ± 2
3rd	39.4 ± 1.9	34 ± 2	31 ± 3	26 ± 3
4th	27 ± 3	21 ± 4	18 ± 4	14 ± 5

2.1. Irradiation setup

The irradiation process was carried out using the high-intensity cyclotron (IBA-C70XP, K = 70) at the GIP ARRONAX research center in Saint-Herblain, France (Haddad et al., 2008). Each stack was placed approximately 6 cm from the end of the beamline, which was sealed with a Kapton layer of 50 μm, and exposed to air. A scintillating Al_2O_3 foil was irradiated to verify that the beam was well-collimated and centered on the stack. The four stacks were irradiated in two separate sessions few months apart: during the first session, the first and second stacks were irradiated for 1 h each, with constant beam currents of 107 and 101 nA, respectively. In the second session, the third and fourth stacks were irradiated for 30 min each, both at a constant beam current of 150 nA. The exit energy from the cyclotron for alpha beam is fixed at 67.4 ± 0.5 MeV. The average beam energies in each foil (as listed in Table 2) were specifically selected to ensure overlapping energy ranges between successive stack irradiations, which helps to identify any inconsistencies in the experimental data by highlighting potential discontinuities in the resulting curves. The energy degradation and straggling of the beam within the target stack were evaluated by simulating the irradiation geometry with the SRIM code (Biersack and Ziegler, 1982). The uncertainty on the mean energy in each foil (δE) was determined by combining the initial uncertainty on the incident beam energy, the energy straggling within the foil, and the uncertainty in the range determination due to the 2% uncertainty on the areal density (ρdx).

The stability of the beam current during irradiation was continuously monitored using a beam dump equipped with a charge integrator. The total charge of the incoming beam was calculated using the values recommended by IAEA for the monitor reactions (Hermanne et al., 2018). The monitor reactions were ^{27}Al(α,x)^{24}Na and/or ^{nat}Ti(α,x)^{51}Cr depending on the energy.

2.2. Measurements

The activity of the produced radionuclides was measured using HPGe detectors, either at GIP ARRONAX on the same day as the irradiations and the following day, and at the Physics Measurement Laboratory at LASA (Segrate, IT) three days post-irradiation due to transportation delays. Each detector underwent calibration: at GIP ARRONAX the calibration of the two n-type HPGe detectors was performed

with two certified radioactive sources, ^{152}Eu and ^{241}Am. At LASA, three n-type detectors were calibrated using ^{152}Eu and ^{133}Ba.

During the measurements, the irradiated targets were placed on top of spacers to minimize dead time, ensuring that the beam entrance side faced the detector crystal in the same geometric configuration used during calibration. The distance ranged between approximately 1 m immediately after the irradiation to 15 cm one week after the irradiation. At GIP ARRONAX, the first measurement session focused on radionuclides with short half-lives, such as ^{60}Cu (half-life of 23.7 min), ^{61}Cu (half-life of 3.339 h) and ^{61}Co (half-life of 1.649 h). In the second session, held at LASA, measurements were concentrated on radionuclides with longer half-lives.

The activity measurements spanned 8 months following the irradiations to track the decay of medium and long-lived radionuclides. Measurement times varied depending on the half-life: short-lived radionuclides were measured from 7 to 90 min, while long-lived radionuclides, such as cobalt isotopes, ^{59}Fe and ^{54}Mn, required measurement periods ranging from 1 h to 7 days. When multiple gamma emissions were used, the average activity at the time of measurement was calculated as the weighted average of the activities measured at each peak. Similarly, the average activity at the end of the bombardment was determined as the weighted average of the values obtained from each repeated measurement. In both cases, the weights were given by the inverse square of the corresponding experimental uncertainties.

Table 3 lists the radionuclides for which cross sections were measured, along with their half-lives, nuclear decay properties, and production reactions (IAEA-NDS, 2025; Verpelli and Abriola, 2011). The gamma lines used for the determination of the activity of each radionuclide are reported in Table 3 as well. The decay data for the relevant cobalt, nickel and copper isotopes were also checked against the evaluated Nuclear Data Sheets (Yang and Huo, 2014; Huo et al., 2011; Bhat, 1998; Basunia, 2018; Browne and Tuli, 2013; Zuber and Singh, 2015), which are consistent with the values adopted in this work.

2.3. Calculation of reaction cross sections and uncertainty propagation

The experimental cross sections for all radionuclides produced in the irradiated cobalt targets were derived from the measured activities at end of bombardment. The cross section at a given energy was calculated using the standard activation formula in Eq. (1) (Colucci et al., 2024):

$$\sigma(E) = \frac{A \cdot M \cdot Z \cdot e}{\rho dx \cdot N_A \cdot Q \cdot \lambda} \cdot G(t_{irr}) \cdot D(t_{count}) \cdot e^{\lambda \cdot t_{cool}} \cdot 10^{27} \quad (1)$$

where E (MeV) is the mean energy of the alpha beam in the target foil, M (mg mol^{-1}) is the atomic weight of cobalt, Z e (C) is the charge of the alpha particle, N_A (mol^{-1}) is the Avogadro number, A (Bq) is the activity, ρdx (mg cm^{-2}) is the mass thickness, Q (C) is the beam charge, λ (s^{-1}) is the decay constant characteristic of each radionuclide, t_{irr} (s) is the irradiation time, t_{count} (s) is the duration of the measurements, t_{cool} (s) is the time between the end of bombardment (EOB) and the start of measurements while the factor 10^{27} converts cm^2 in mb. The activity A is determined as $\frac{C}{LT \cdot \epsilon \cdot I_\gamma}$, where C are the net counts of the photo-peak of energy E, I_γ is the abundance of the gamma emission of energy E, ϵ is the detector efficiency at energy E and LT (s) is the Live Time of the measurement, given by the time of measurements without dead time. Two multiplicative factors are also present: the growing factor $G(t_{irr})$ which takes into account the decay of the produced radionuclide during the irradiation, and the decay factor $D(t_{count})$ which corrects for the decay of the radionuclides during the measurements:

$$G(t_{irr}) = \frac{\lambda \cdot t_{irr}}{1 - e^{-\lambda t_{irr}}}$$
$$D(t_{count}) = \frac{\lambda \cdot t_{count}}{1 - e^{-\lambda t_{count}}} \quad (2)$$

The uncertainties on the cross-section values were evaluated through standard error-propagation formulas, taking into account the uncertainties of the relevant physical quantities. In the case of the cross section, the absolute uncertainty ϵ_σ has been estimated by using the following Equation:

$$\epsilon_\sigma = \sqrt{\left(\frac{\epsilon_A}{A}\right)^2 + \left(\frac{\epsilon_{\rho dx}}{\rho dx}\right)^2 + \left(\frac{\epsilon_Q}{Q}\right)^2} \cdot \sigma \quad (3)$$

where ϵ_i is the uncertainty on the ith quantity. The uncertainty on the mass thickness ($\epsilon_{\rho dx}/\rho dx$) was set to 2%, as stated above. The uncertainty on the collected charge (ϵ_Q/Q) ranged from 1.2% to 2.5%, depending on the stack. It was derived from the uncertainty on the activity measured for the monitor foils, combined with the uncertainty associated with the recommended cross-section data of the monitor reactions. An average beam charge was determined using several monitor foils and different monitor reactions in order to minimize the overall uncertainty. The uncertainty on the activity A is determined using the following Equation:

$$\epsilon_A = \sqrt{\left(\frac{\epsilon_{CPS}}{CPS}\right)^2 + \left(\frac{\epsilon_{I_\gamma}}{I_\gamma}\right)^2 + \left(\frac{\epsilon_\varepsilon}{\varepsilon}\right)^2} \cdot A \quad (4)$$

where CPS is defined as $\frac{C}{LT}$. LT has been set so that the counting statistics is good enough to ensure a counting uncertainty generally lower than 10%. The uncertainty in the gamma-ray intensity, ϵ_{I_γ}, is sourced from the IAEA database (IAEA-NDS, 2025), while the relative uncertainty in detector efficiency is lower than 3% and depends on the energy. The relative uncertainty on the beam charge is determined by propagating the measurement uncertainties on the recommended data sourced from IAEA (Hermanne et al., 2018). Multiple measurements allow to reduce the uncertainty on the cross sections that ranges from 4% to 30%.

When repeated measurements are performed or multiple peaks are used to determine the activity of a single radionuclide the uncertainty on the weighted average is determined as the maximum between:

$$\epsilon = \sqrt{\frac{1}{\sum_i \epsilon_i^{-2}}} \quad (5)$$

and

$$\epsilon = \sqrt{\frac{\sum_i (x_i - \mu)^2 \cdot \epsilon_i^{-2}}{\sum_i \epsilon_i^{-2}}}. \quad (6)$$

where μ is the weighted average value, x_i is the ith repetition of the measurement (or the ith peak) and ϵ_i is the standard uncertainty of x_i (Gilmore, 2008). The symbol ϵ is here used in a general sense to indicate the uncertainty on the averaged quantity, which can correspond either to repeated measurements of the same peak or to the average activity obtained from multiple peaks of the same radionuclide.

3. Results and discussion

The experimental cross-section values obtained in this work are summarized in Tables 4 and 5.

The corresponding excitation functions are displayed in Figs. 2–10, where they are compared with previously published experimental datasets (Ansari et al., 2004; Gadioli et al., 1984; Homma and Murakami, 1976, 1977; Ismail and Divatia, 1988; Ismail, 1993; Jastrzębski et al., 1986; Michel and Brinkmann, 1980; Mukherjee et al., 1998; Neuzil and Lindsay, 1963; Rama Rao et al., 1987; Singh et al., 1993; Skulski et al., 1992; Szelecsényi et al., 2002; Zhukova et al., 1972; Stearns, 1962; Levkovskij, 1991), and with the computer simulations TALYS 1.96 (Koning and Hilaire, 2023) run with default settings.

Table 3
Gamma emissions used for the determination of cross sections of produced radionuclides with their abundances. Uncertainties are reported in italic and refer to the last significant digits (IAEA-NDS, 2025; Verpelli and Abriola, 2011).

Nuclide	Half-life	Nuclear reaction	E_{th} (MeV)	E_γ (keV)	I_γ (%)
^{61}Cu	3.339 *7* h	(α, 2n)	14.8	282.956 *10*	12.7 *20*
EC, β^+ (100)				373.050 *10*	2.1 *3*
				656.008 *10*	10.4 *16*
				1185.234 *15*	3.6 *6*
^{60}Cu	23.7 *4* m	(α, 3n)	27.2	467.3 *2*	3.52 *18*
EC, β^+ (100)				497.9 *2*	1.67 *9*
				826.4 *2*	21.7 *11*
				952.4 *2*	2.73 *18*
				1035.2 *2*	3.70 *18*
				1293.7 *2*	1.85 *18*
^{56}Co	77.236 *26* d	(α, 3n α)	32.2	846.770 *2*	99.9399 *23*
EC, β^+ (100)		(α, n 2t)	44.3	1037.843 *4*	14.05 *4*
		(α, 2n d t)	50.9	1238.288 *3*	66.46 *12*
		(α, 3n p t)	53.3	1360.212 *4*	4.28 *12*
		(α, 4n ^{3}He)	54.1		
		(α, 3n 2d)	57.5		
^{57}Co	271.74 *6* d	(α, 2n α)	20.2	122.06065 *12*	85.60 *17*
EC (100)		(α, 2t)	32.2	136.4736 *3*	10.68 *8*
		(α, n d t)	38.8		
^{58}Co	70.86 d *6*	(α, n α)	11.1	810.7593 *20*	99.45 *1*
EC, β^+ (100)		(α, d t)	29.7	863.951 *6*	0.686 *10*
		(α, n p t)	32.1		
		(α, 2n ^{3}He)	32.9		
		(α, n 2d)	36.4		
		(α, 2n p d)	38.7		
^{60}Co	1925.28 *14* d	(α, ^{3}He)	13.9	1332.492 *4*	99.9826 *6*
β^- (100)		(α, p d)	19.7		
		(α, n 2p)	22.1		
^{61}Co	1.649 *5* h	(α, 2p)	12.2	67.412 *10*	84.7 *4*
β^- (100)					
^{59}Fe	44.490 *9* d	(α, p ^{3}He)	22.7	1099.245 *3*	56.5 *9*
β^- (100)		(α, 2p d)	28.5	1291.590 *6*	43.2 *9*
		(α, n 3p)	30.8		
^{54}Mn	312.20 *20* d	(α, n 2α)	18.2	834.848 *3*	99.976 *1*
EC, β^+ (100)		(α, d t α)	36.9		
		(α, n p t α)	39.2		
		(α, 2n ^{3}He α)	40.0		
		(α, n 2d α)	43.5		
		(α, 2n p d α)	45.9		
		(α, 3n 2p α)	48.2		
		(α, 2t ^{3}He)	52.0		
		(α, p d 2t)	57.9		
		(α, 2n d t ^{3}He)	58.7		

Table 4
Values of the cross sections σ, with their respective uncertainties ϵ_σ, of the short-lived radionuclides measured at ARRONAX. The average beam energy E and energy uncertainty δE in each target are also presented.

E (MeV)	^{61}Cu (mb)	^{60}Cu (mb)	^{61}Co (mb)
58.7 ± 1.0	21.4 ± 1.1	27 ± 2	3.5 ± 0.2
56.2 ± 1.1	24.7 ± 1.4	36 ± 3	3.81 ± 0.17
53.6 ± 1.2	29.6 ± 1.8	48 ± 4	4.16 ± 0.17
50.8 ± 1.4	31 ± 2	50 ± 3	3.9 ± 0.4
48.2 ± 1.5	43.0 ± 1.9	68 ± 4	4.7 ± 0.2
45.5 ± 1.6	56 ± 3	68 ± 4	5.1 ± 0.4
43.3 ± 1.8	71 ± 3	66 ± 3	5.7 ± 0.4
39.4 ± 1.9	145 ± 8	55 ± 3	8.6 ± 0.4
39 ± 2	142 ± 6	42 ± 2	7.4 ± 0.3
34 ± 2	305 ± 14	14.5 ± 0.9	9.6 ± 0.4
31 ± 3	374 ± 19	3.3 ± 0.3	9.6 ± 0.4
27 ± 3	510 ± 20	–	3.7 ± 0.5
26 ± 3	450 ± 30	–	1.7 ± 0.6
21 ± 4	310 ± 15	–	–
17 ± 4	98 ± 4	–	–
14 ± 5	3.1 ± 0.3	–	–

3.1. $^{59}Co(\alpha,2n)^{61}Cu$

The production cross sections of ^{61}Cu are shown in Fig. 2. The excitation function is a peak-shaped curve, with a maximum around 28 MeV and a long tail at high energies. The cross sections values are high (σ_{max} = 507 mb); therefore, a high production yield for ^{61}Cu is expected. The data from other works are in accordance with the measurements of this work and follow the same general trend, except for Homma and Murakami (1976), Ansari et al. (2004) and Zhukova et al. (1972), which seem to underestimate the data in the peak region. The TALYS 1.96 seems to be shifted to lower energies, not accurately reproducing the experimental results. The measurements used to estimate ^{61}Cu were carried out the first two days after the end of the irradiation at the GIP ARRONAX research center due to the relatively short half-life of this radionuclide ($T_{1/2}$ = 3.339 h).

The intensity of the 656 keV gamma emission from this radionuclide was re-evaluated by Bleuel et al. (2021), suggesting a reduction from the previously accepted value of 10.4 ± 1.6% reported in IAEA-NDS (2025) to 9.7 ± 1.7%. In this work, we adopted the former value for consistency with other datasets. In our case, the potential systematic

Table 5
Values of the cross sections σ, with their respective uncertainties ϵ_σ, of the long-lived radionuclides measured at LASA. The average beam energy E and energy uncertainty δE in each target are also presented.

E (MeV)	^{56}Co (mb)	^{57,cum}Co (mb)	$^{58g+m}$Co (mb)	^{60,cum}Co (mb)	^{59}Fe (mb)	^{54}Mn (mb)
58.7 ± 1.0	49 ± 2	111 ± 4	130 ± 6	53 ± 2	1.55 ± 0.14	25.4 ± 1.2
56.2 ± 1.1	41.8 ± 1.6	134 ± 5	117 ± 5	59 ± 2	1.10 ± 0.08	29.9 ± 1.2
53.6 ± 1.2	29.6 ± 1.2	161 ± 6	108 ± 5	64 ± 3	0.67 ± 0.06	32.0 ± 1.2
50.8 ± 1.4	14.4 ± 0.7	167 ± 5	96 ± 4	62 ± 3	0.35 ± 0.05	27.7 ± 1.1
48.2 ± 1.5	6.4 ± 0.4	192 ± 7	106 ± 5	66 ± 3	0.16 ± 0.03	26.0 ± 1.1
45.5 ± 1.6	1.64 ± 0.10	197 ± 6	118 ± 5	62 ± 3	0.163 ± 0.016	19.9 ± 0.7
43.3 ± 1.8	0.27 ± 0.02	179 ± 6	129 ± 5	52 ± 2	0.13 ± 0.02	13.0 ± 0.6
39.4 ± 1.9	–	153 ± 6	172 ± 8	36.9 ± 1.7	0.091 ± 0.006	4.5 ± 0.3
39 ± 2	0.05 ± 0.02	127 ± 5	173 ± 9	28 ± 2	0.083 ± 0.013	2.7 ± 0.2
34 ± 2	–	57 ± 2	231 ± 10	11.0 ± 0.8	0.060 ± 0.012	–
31 ± 3	–	16.6 ± 1.1	228 ± 11	3.7 ± 0.6	–	–
27 ± 3	–	1.4 ± 0.5	228 ± 12	–	–	–
26 ± 3	–	0.67 ± 0.19	185 ± 8	4.1 ± 1.6	–	–
21 ± 4	–	1.4 ± 0.2	95 ± 4	–	–	–
18 ± 4	–	–	15.7 ± 0.7	–	–	–
14 ± 5	–	–	1.50 ± 0.17	–	–	–

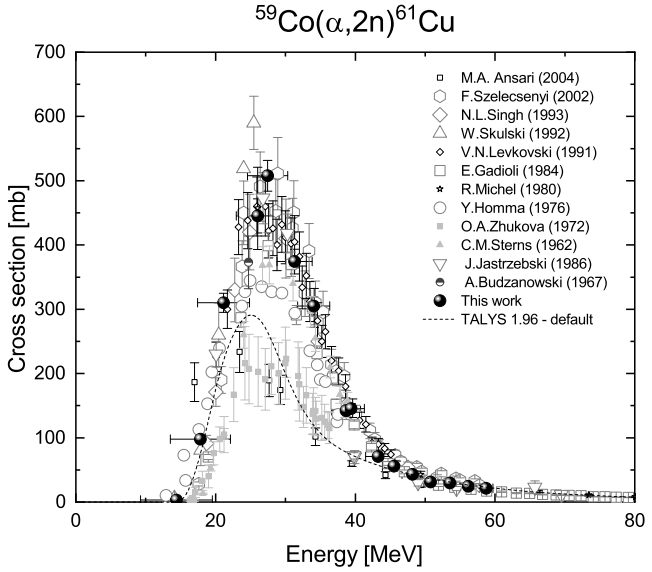

Fig. 2. Experimental cross section of ^{59}Co(α,2n)^{61}Cu reaction in comparison with TALYS 1.96 simulation and previous experimental results (Szelecsényi et al., 2002; Singh et al., 1993; Skulski et al., 1992; Gadioli et al., 1984; Homma and Murakami, 1976; Jastrzębski et al., 1986; Ansari et al., 2004; Michel and Brinkmann, 1980; Zhukova et al., 1972; Stearns, 1962; Levkovskij, 1991; Budzanowski et al., 1967).

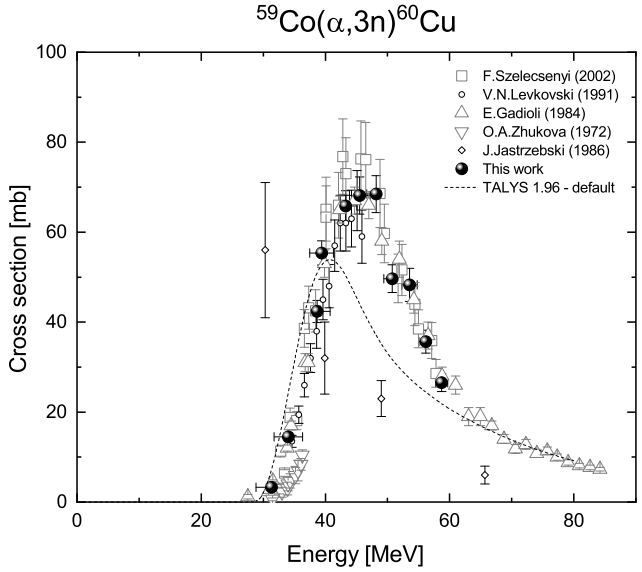

Fig. 3. Experimental cross section of ^{59}Co(α,3n)^{60}Cu reaction in comparison with TALYS 1.96 simulation and previous experimental results (Szelecsényi et al., 2002; Gadioli et al., 1984; Levkovskij, 1991; Zhukova et al., 1972; Jastrzębski et al., 1986).

deviation introduced by this choice was not found to significantly impact the results, as the associated uncertainty exceeds the possible bias introduced by the intensity difference. This is consistent with a recent re-evaluation of ^{61}Cu cross sections (Hermanne et al., 2025), where updated gamma-ray intensities—based on (IAEA-NDS, 2025) and the ratio proposed by Bleuel et al. (2021) were applied to selected datasets. The resulting corrections led to variations of only 2%–6% in the cross section values, well within the typical experimental uncertainties.

3.2. ^{59}Co(α,3n)^{60}Cu

The excitation function for the production of ^{60}Cu ($T_{1/2}$ = 23.7 m) is reported in Fig. 3. The energy threshold of the reaction ^{59}Co(α,3n)^{60}Cu is 27.2 MeV (IAEA-NDS, 2025). Consequently, no ^{60}Cu can be seen in the fourth stack as the irradiation energy there falls below 30 MeV. Notably, the production of ^{60}Cu, the primary contaminant of ^{61}Cu, ceases before reaching the maximum cross section value for ^{61}Cu production. This observation suggests that ^{61}Cu can be produced without ^{60}Cu contamination by selecting an appropriate energy range, a point that will be elaborated on later. The data in this work are aligned well with previous studies. Data clearly show that results from Jastrzębski et al. (1986) should not be considered as they are clearly off the other datasets. Simulations performed with TALYS 1.96 tend to underestimate the experimental excitation functions considered in this work. Measurements used to estimate ^{60}Cu were performed on the first and second days after the end of irradiation at the GIP ARRONAX research center, due to the short half-life of this radionuclide ($T_{1/2}$ = 23.7 min).

3.3. ^{59}Co(α,x)^{56}Co

The excitation function for the production of ^{56}Co ($T_{1/2}$ = 77.2 d (IAEA-NDS, 2025)) is shown in Fig. 4. Here, it can be seen that the data from this work align well with previous studies, except for the three experimental points around 40 MeV of Ansari et al. (2004) and Ismail (1993). These datasets have already been identified as possibly problematic for the production of ^{61}Cu. TALYS 1.96 simulation reproduces the overall trend of the experimental data in this work with a shift to lower energies. ^{56}Co energy threshold is 32.2 MeV (IAEA-NDS,

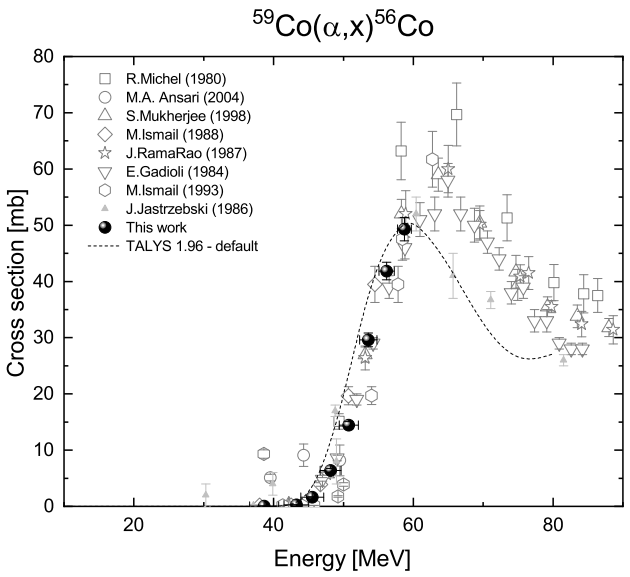

Fig. 4. Experimental cross section of ^{59}Co(α,x)^{56}Co reaction in comparison with TALYS 1.96 simulation and previous experimental results (Michel and Brinkmann, 1980; Ansari et al., 2004; Mukherjee et al., 1998; Ismail and Divatia, 1988; Rama Rao et al., 1987; Gadioli et al., 1984; Ismail, 1993; Jastrzębski et al., 1986).

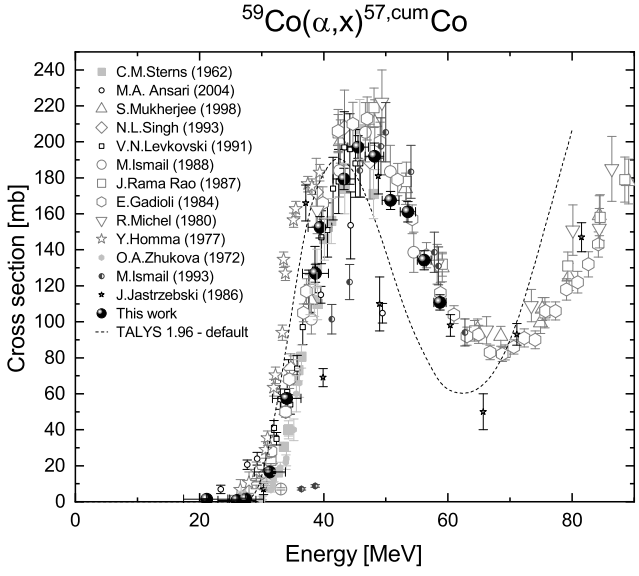

Fig. 5. Experimental cross section of ^{59}Co(α,x)^{57,cum}Co reaction in comparison with TALYS 1.96 simulation and previous experimental results (Mukherjee et al., 1998; Singh et al., 1993; Ismail and Divatia, 1988; Rama Rao et al., 1987; Gadioli et al., 1984; Michel and Brinkmann, 1980; Homma and Murakami, 1977; Stearns, 1962; Ansari et al., 2004; Levkovskij, 1991; Zhukova et al., 1972; Jastrzębski et al., 1986). The production of ^{57}Co is cumulated from the possible contribute of the decay of ^{57}Ni above 46 MeV.

2025), however, this radionuclide was not observed below 38.7 MeV probably due to the fact that only one reaction channel (α,3n) has an energy threshold below this value and its cross section is low.

3.4. ^{59}Co(α,2p)^{57,cum}Co

The excitation function of the reaction ^{59}Co(α,x)^{57,cum}Co ($T_{1/2}$ = 272 d (IAEA-NDS, 2025)) is shown in Fig. 5. No gamma-lines attributable to the decay of the precursor ^{57}Ni ($T_{1/2}$ = 35.6 h), in

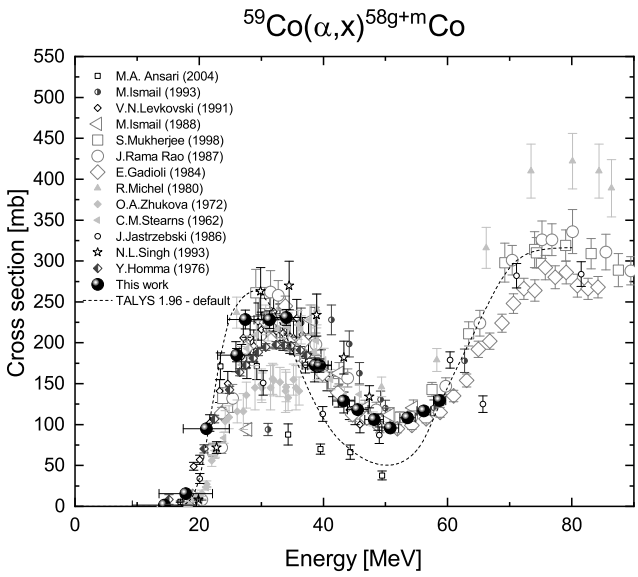

Fig. 6. Experimental cross section of ^{59}Co(α,x)$^{58g+m}$Co reaction in comparison with TALYS 1.96 simulation and previous experimental results (Ismail and Divatia, 1988; Mukherjee et al., 1998; Rama Rao et al., 1987; Gadioli et al., 1984; Ansari et al., 2004; Stearns, 1962; Michel and Brinkmann, 1980; Levkovskij, 1991; Zhukova et al., 1972; Jastrzębski et al., 1986; Singh et al., 1993; Homma and Murakami, 1977; Ismail, 1993). The production of ^{58}Co is cumulated with the contribute of the decay of the metastable state ^{58m}Co.

particular the 368.7 keV transition (35.3%), were observed in our spectra, indicating that its production is below our detection capability. However, given the reaction threshold near 46 MeV and the fact that ^{57}Ni can decay to ^{57}Co via electron capture, a small contribution cannot be excluded. For this reason, the ^{57}Co cross sections are reported as cumulative, and only spectra registered after 30 days from EOB were considered for the determination of the cross-section.

In Fig. 5, it can be seen that the data from other works align well with those from this work. As in the case of ^{61}Cu and ^{56}Co, exceptions are represented by Jastrzębski et al. (1986) whose data are strongly scattered, the data of Ansari et al. (2004) at energies greater than 40 MeV and the data of Ismail (1993) that appear shifted to higher energies of about 5 MeV . In this case, the data of Homma and Murakami (1977) seem to be shifted to lower energies. The TALYS 1.96 simulation reproduces well the data below 40 MeV.

3.5. ^{59}Co(α,x)^{58}Co

^{58}Co has a metastable state ($T_{1/2}$ = 9.10 h (IAEA-NDS, 2025)) that decay by IT in the ground state ^{58g}Co ($T_{1/2}$ = 70.9 d (IAEA-NDS, 2025)) with a 100% branching ratio. However the quantification of the activity of the metastable state is complex since its only gamma emission has low energy (E_γ = 25.889 keV) and low intensity (I_γ = 0.0397%). The excitation function for the production of ^{58}Co is therefore reported as cumulated in Fig. 6. The activity measurements started one week after the EOB. Here, it can be seen that the data in this work align well with most of the data present in literature: results from Zhukova et al. (1972), Homma and Murakami (1977) and Ansari et al. (2004) tend to underestimate the excitation function in the whole studied range, the data of Ismail (1993) that appear shifted to higher energies of about 5 MeV. The data from Singh et al. (1993) overestimate the cross-sections in the maximum region. The TALYS 1.96 simulation include the contribute of the IT, but it does not reproduce the trend very well for all energies.

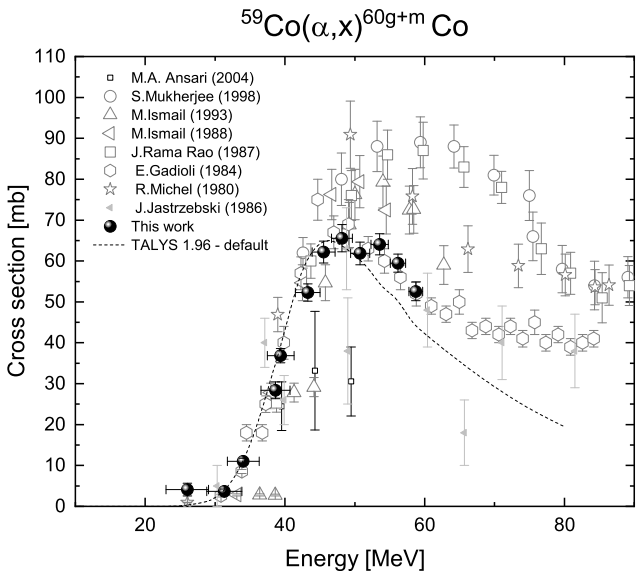

Fig. 7. Experimental cross section of ^{59}Co(α,x)^{60,cum}Co reaction in comparison with TALYS 1.96 simulation and previous experimental results (Mukherjee et al., 1998; Ismail, 1993; Ismail and Divatia, 1988; Rama Rao et al., 1987; Gadioli et al., 1984; Michel and Brinkmann, 1980; Ansari et al., 2004; Jastrzębski et al., 1986). The production of ^{60}Co is cumulated with the contribute of the decay of the metastable state ^{60m}Co.

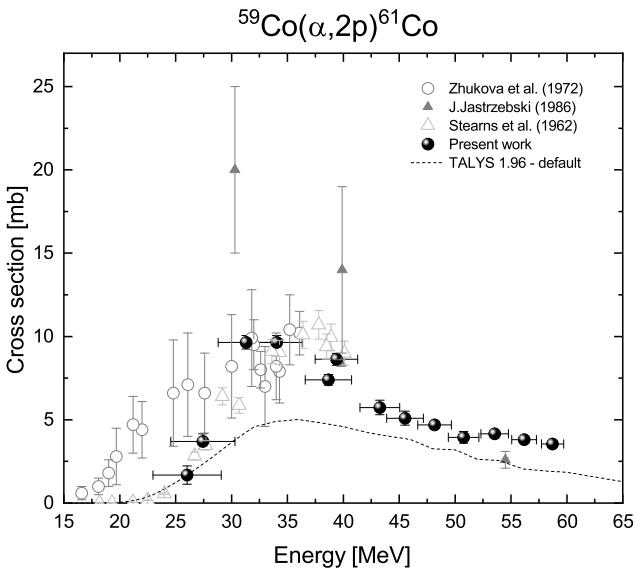

Fig. 8. Experimental cross section of ^{59}Co(α,x)^{61}Co reaction in comparison with TALYS 1.96 simulation and previous experimental results (Zhukova et al., 1972; Stearns, 1962).

3.6. $^{59}Co(\alpha,x)^{60}Co$

The cross sections for the production of ^{60}Co ($T_{1/2}$ = 1925 d (IAEA-NDS, 2025)) are shown in Fig. 7. It is not possible to exclude the contribute of the metastable state ^{60m}Co ($T_{1/2}$ = 10.467 min (IAEA-NDS, 2025), IT = 99.76%) since its gamma emission (E_γ = 58.6 keV, I_γ = 2.07%) is hard to be detected, therefore the cross section is reported as cumulated. Spectra acquired before one week from the EOB were not considered in the determination of the activity of ^{60}Co. Excluding data from the work of Ansari et al. (2004) and Jastrzębski et al. (1986), there is good agreement between experimental results below 50 MeV. Above this energy, the literature data present two different trends: one trend shows lower cross section values, while the other shows higher values. Data from this work follow the trend found by Gadioli et al. (1984). ^{60}Co has two gamma emissions: one at 1332 keV with an intensity of 99.98%, and another at 1173 keV with an intensity of 99.97%. The latter gamma emission overlaps with the ^{56}Co gamma emission at 1175 keV, which has an abundance of 2.252%. This superposition of gamma emission is likely not considered by other authors in determining the cross section of production of ^{60}Co, with a consequent increase of the measured cross section. In the present work only the emission at higher energy has been used to determine the production cross section. The TALYS 1.96 simulation reproduces the trend very well for energies below 50 MeV, and above 50 MeV it seems to follow the trend towards lower values. The energy threshold for ^{60}Co is 13.9 MeV (IAEA-NDS, 2025). However, the cross sections for the fourth stack could not be determined because of the suppression caused by the Coulomb barrier below 23 MeV.

3.7. $^{59}Co(\alpha,x)^{61}Co$

The cross sections for the production of ^{61}Co ($T_{1/2}$ = 1.649 h (IAEA-NDS, 2025)) are reported in Fig. 8. The gamma ray used for the determination of the activity of ^{61}Co in this work is the one at 67.412 keV (I_γ = 84.7%) is also present in the emission spectrum of ^{61}Cu but with lower intensity (I_γ = 4.0%). The latter contribution have been subtracted accordingly. As a verification, the decay time of ^{61}Co has been measured, obtaining an experimental value of $T_{1/2}^{exp}$ = 1.62 ± 0.02 h, that is in very good agreement with the one reported in literature.

There is good agreement between the experimental results of this work and the data of Zhukova et al. (1972). The data of Stearns (1962) seem to overestimate the cross section at low energies. No experimental results are available at energies higher than 40 MeV. The TALYS 1.96 simulation underestimates the cross section in the whole energy range, the data from (Jastrzębski et al., 1986) exhibit great uncertainty between 30 and 40 MeV.

3.8. $^{59}Co(\alpha,x)^{59}Fe$

The cross sections for the production of ^{59}Fe ($T_{1/2}$ = 44.490 d (IAEA-NDS, 2025)) are presented in Fig. 9. There is a good agreement between the experimental results of this work with data from the literature in the energy range investigated in this work. The TALYS 1.96 simulation has the same trend of the experimental data below 60 MeV and then it reproduces data from the work of Gadioli et al. (1984) at higher energy.

3.9. $^{59}Co(\alpha,x)^{54}Mn$

The production cross sections of ^{54}Mn ($T_{1/2}$ = 312 d (IAEA-NDS, 2025)) are reported in Fig. 10. There is a good agreement between the experimental results of this work and the data in the literature. Few datasets are off, but they are the same as the one that presents discrepancies for other radionuclides studied in this work. The TALYS 1.96 simulations tend to underestimate the trend of cross section's values.

4. Optimization of the production of ^{61}Cu

To optimize the production of a radionuclide it is necessary to determine the produced activity of the radionuclide of interest and of all the co-produced contaminants as a function of the parameters of irradiations, including the entrance energy, the thickness of the target and the irradiation time.

The Physical Thick Target Yield, α_{phys} (MBq C^{-1}), for all produced radionuclides was calculated using the following formula (Otuka and Takács, 2015; Pupillo et al., 2022):

$$\alpha_{phys}(E;\Delta E) = \frac{N_A \cdot \lambda}{M \cdot Ze} \int_{E-\Delta E}^{E} \frac{\sigma(E')}{\frac{1}{\rho}\frac{dE}{dx}(E')} dE' \quad (7)$$

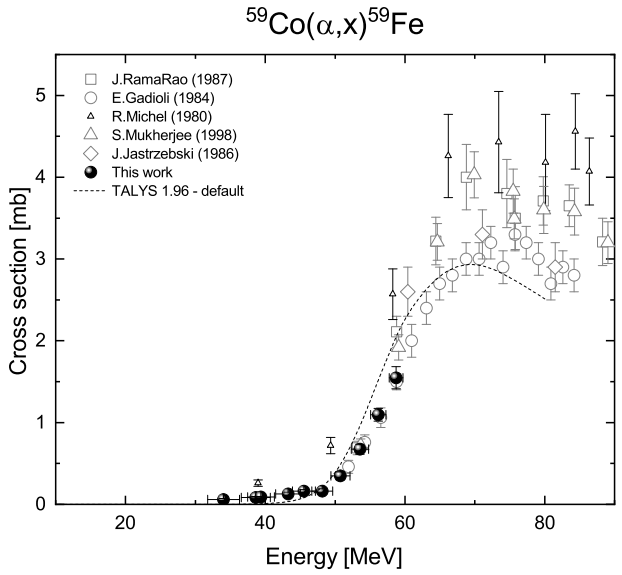

Fig. 9. Experimental cross section of ^{59}Co(α,x)^{59}Fe reaction in comparison with TALYS 1.96 simulation and previous experimental results (Rama Rao et al., 1987; Gadioli et al., 1984; Mukherjee et al., 1998; Jastrzębski et al., 1986; Michel and Brinkmann, 1980).

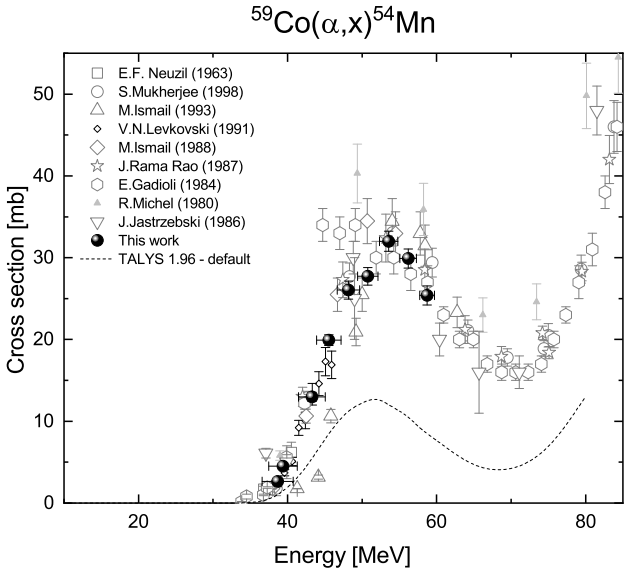

Fig. 10. Experimental cross section of ^{59}Co(α,x)^{54}Mn reaction in comparison with TALYS 1.96 simulation and previous experimental results (Neuzil and Lindsay, 1963; Mukherjee et al., 1998; Ismail, 1993; Ismail and Divatia, 1988; Rama Rao et al., 1987; Gadioli et al., 1984; Jastrzębski et al., 1986; Michel and Brinkmann, 1980; Levkovskij, 1991).

where E is the incident alpha beam energy, ΔE is the energy loss within the thick target, and $\frac{1}{\rho}\frac{dE}{dx}$ is the mass stopping power of α particles in the target material. The terms N_A, M, λ, Z and e are defined in Eq. (1). The α_{phys} for the produced radionuclides is reported in Fig. 11.

The activity produced per unit of current at the EOB, namely the Thick Target Yield TTY^{EOB} (MBq μA^{-1}), depends non linearly on the duration of the irradiation and it is related to α_{phys} through the relation (Otuka and Takács, 2015):

$$TTY^{EOB}(E;\Delta E;t_{irr}) = \frac{1-e^{-\lambda t_{irr}}}{\lambda}\cdot\alpha_{phys}(E,\Delta E) \quad (8)$$

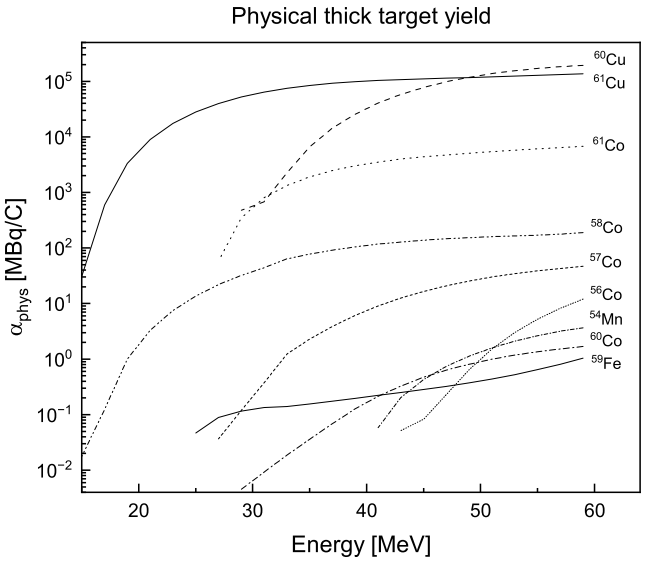

Fig. 11. α_{phys} of ^{61}Cu and its contaminants as a function of the incident α beam energy and for various energy losses ΔE. The graph refers to the condition of complete absorption of the beam within the target.

The production of a specific radionuclide reaches saturation as the duration of irradiation approaches eight half-lives (Loveland et al., 2006). In the case of ^{61}Cu ($T_{1/2}$ = 3.339 h (IAEA-NDS, 2025)) the saturation is reached after approximately 22 h. For the production of ^{61}Cu via the ^{59}Co(α,2n) reaction, an irradiation time of 3 h was selected. This corresponds to approximately one half-life of ^{61}Cu. After this irradiation period, the saturation yield reaches 46%, and the activity growth still exhibits an almost linear trend. In these conditions, the maximum TTY^{EOB} is of about 1.1 GBq μA^{-1} when the entrance energy of the alpha beam is 59 MeV and energy losses of 44 MeV (down to the threshold energy of production of ^{61}Cu). To ensure an energy loss of 44 MeV a Co mass thickness of 370 mg cm^{-2} is required, which is equivalent to a physical thickness of 430 μm considering a metal target with density 8.6 g cm^{-3}.

At the same pair (E; ΔE) = (59 MeV; 44 MeV) for an irradiation of 3 h, the TTY^{EOB} of ^{60}Cu, is 400 MBq μA^{-1}, while the TTY^{EOB} of ^{62}Cu have been estimated to be approximately 1.8 GBq μA^{-1} from the literature data (Szelecsényi et al., 2002; Skulski et al., 1992; Jastrzębski et al., 1986; Zhukova et al., 1972; Stearns, 1962). The latter radionuclide could not be measured in this work due to its short half-life of 9.67 min and the very low intensities of its gamma emissions (IAEA-NDS, 2025). Considering that ^{60}Cu has a half-life of 23.7 min and ^{62}Cu has a half-life of 9.67 min, waiting for the decay of these contaminants, it is possible to achieve a RNP above 99.9% for this pair (E; ΔE) in 4 h with a reduction of the activity of ^{61}Cu to 480 MBq μA^{-1}.

From Fig. 11 it is possible to extract different interesting features. The most important one is that the ratio between the yield of ^{61}Cu and ^{60}Cu increases while decreasing the entrance energy down to about 30 MeV. Moreover the yield of production of the non-isotopic contaminants is orders of magnitude lower than the one of ^{61}Cu. This is mainly due to the fact that all of them have half-lives much longer than the one of ^{61,60}Cu. It is possible to chemically remove these contaminants in an effective way using different radiochemical methods (Das et al., 2012; Sadeghi et al., 2008). This characteristic is significant for the RNP and Specific Activity of the final product, even though their presence must be taken into account when dealing with waste disposal, making their reduction advisable.

Based on the cross section data, it is interesting to evaluate the production of ^{61}Cu in the range 45–20 MeV, completely covering the peak of production of this radionuclide. In this case, with an irradiation

Table 6
Comparison between irradiation at 59 MeV, 45 MeV and 30 MeV. The duration of the irradiation is fixed at 3 h. Metal Co targets have been considered. t_d is the waiting time after the EOB.

E (MeV)	ΔE (MeV)	t_d (h)	TTY^{EOB} (MBq μA^{-1})	TTY(t_d) (MBq μA^{-1})	RNP(t_d) (%)	ρdx (mg cm^{-2})	Thickness (μm)
59	44	4.0	1100	480	99.9	370	430
45	25	3.4	840	420	99.9	195	226
30	10	1.8	420	290	99.9	65	76

time of 3 h, the TTY^{EOB} of ^{61}Cu is about 840 MBq μA^{-1}, while the ones of ^{62}Cu and ^{60}Cu are 850 MBq μA^{-1} and 150 Bq μA^{-1} respectively. A RNP of 99.9% can be reached after a waiting time of 3.4 h, obtaining 420 MBq μA^{-1} of pure ^{61}Cu. The mass thickness of the target required to degrade the energy of the beam from 45 to 20 MeV is 195 mg cm^{-2} corresponding to a thickness of 226 μm.

Nowadays, there is a growing interest in installing new α-accelerators with energies up to 30 MeV for the production of medical radionuclides. In particular, these accelerators are valuable for producing ^{211}At, a promising alpha emitter for targeted alpha therapy (Qaim, 2024; Aliev et al., 2023). It is therefore useful to evaluate the possibility to exploit this kind of accelerator to produce other radionuclides for medical applications.

Considering an optimal irradiation time of 3 h, the maximum TTY^{EOB} for ^{61}Cu in conditions of complete absorption of the beam within the target reaches 470 MBq μA^{-1}. However, reducing the energy loss to 10 MeV (exit energy 20 MeV as in the hypothesis discussed above) results in a slightly lower activity of 420 MBq μA^{-1}, while minimizing the amount of irradiated material. Under irradiation conditions of (E; ΔE; t_{irr}) = (30 MeV; 10 MeV; 3 h), the TTY^{EOB} values for the isotopic contaminant ^{62}Cu is 350 MBq μA^{-1}, while the production of ^{60}Cu is negligible (below 100 kBq μA^{-1}). A radionuclide purity (RNP) exceeding 99.9% is achieved after 1.8 h, corresponding to 11 half-lives of ^{62}Cu, reaching a final activity of ^{61}Cu of 290 MBq μA^{-1}. Additionally, at 30 MeV, the required amount of cobalt target material is significantly reduced: a mass thickness of 65 mg cm^{-2} is sufficient to degrade the energy from 30 MeV to 20 MeV, and it corresponds to a physical thickness of 76 μm.

In Table 6, the comparison between the activity per unit of current of ^{61}Cu produced at 30 MeV, 45 MeV and 59 MeV is reported, alongside with the reached RNP and the thicknesses of cobalt required.

4.1. Practical implications

The proposed production route offers several advantages for routine clinical supply of ^{61}Cu:

- Cost-effectiveness: cobalt is monoisotopic and inexpensive compared to enriched Zn or Ni targets, simplifying radiochemical separation;
- Compatibility with emerging accelerators: 30 MeV α-accelerators, primarily developed for ^{211}At, can also produce ^{61}Cu with acceptable yields and purity, enabling multi-isotope production platforms;
- Reduced waste and target thickness: lower entrance energy (30 MeV) requires only ∼ 76 μm Co thickness, minimizing material costs and radioactive waste;
- High radionuclidic purity: RNP >99.9% achievable after short decay times (≤2 h for 30 MeV), ensuring clinical-grade product without complex purification steps.

These features make the ^{59}Co(α,2n)^{61}Cu reaction a practical alternative for PET imaging radionuclide supply in hospital-based or regional production facilities.

5. Potential use of ^{59}Co(α,x) reactions for monitor purposes

The list of monitor reactions for charged particles has been recently extended (Tárkányi et al., 2024); however, ^{59}Co has not yet been considered as a possible monitor target in the stacked-foil technique. Nevertheless, several of the radionuclides produced through the ^{59}Co(α,x) reactions are already included in the monitor list when produced via different nuclear reactions (e.g.,^{nat}Ni(α,x)^{60,61}Cu,^{57}Co, or ^{nat}Cu(p,x)^{61}Cu,^{56,58}Co, etc. Hermanne et al. (2018), Tárkányi et al. (2024)).

The results obtained in this work demonstrate that several nuclear reactions induced by α-particles on ^{59}Co targets show promising features for use as monitor reactions in alpha beam irradiations. Three advantages support this potential application:

- **Wide range of half-lives:** The radionuclides produced exhibit half-lives ranging from minutes to hundreds of days. This wide variety allows flexible measurement times after the EOB, enabling different radionuclides to be analyzed on the same monitor foil at optimized times without overlap.
- **Consistency across multiple studies:** The excitation functions of the main reaction products have been measured by several independent groups, showing good mutual agreement, particularly for ^{61}Cu,^{60}Cu, ^{56}Co, ^{57}Co, ^{58}Co, and ^{54}Mn. This cross-validation enhances the reliability of using these reactions for monitoring purposes. Exceptions are the datasets of Jastrzębski et al. (1986) and Ansari et al. (2004), whose cross sections frequently deviate from the results reported by other studies.
- **Multiple gamma emissions:** Many of the produced radionuclides emit several gamma lines with significant intensities. This enables the activity to be determined by averaging results from multiple gamma peaks, reducing the impact of potential interferences or spectral overlaps, and ensuring more robust and accurate measurements.

A potential drawback, compared to most of the currently recommended monitor reactions, is that pure cobalt foils are typically more expensive than alternative target materials such as natural aluminum, nickel, titanium, or copper.

6. Conclusions

This study investigated the production of ^{61}Cu via the ^{59}Co(α,2n) reaction by measuring its excitation function in the energy range of 14–59 MeV. The cross section data were obtained using the stacked-foil technique and compared with previous experimental data and theoretical calculations from TALYS 1.96. Our results confirm that ^{61}Cu can be efficiently produced using medium-energy α-particle beams, with a maximum cross section of 510 mb at approximately 27 MeV.

TTY and RNP calculations were performed to identify optimal irradiation conditions. We found that using an incident energy of 45 MeV with a 25 MeV energy loss (down to 20 MeV) and a 3-hour irradiation yields a TTY^{EOB} of 840 MBq μA^{-1}. After a 3.4 h post-irradiation decay, a final yield of 420 MBq μA^{-1} with a RNP exceeding 99.9% can be obtained. This approach provides high production efficiency while minimizing the impact of short-lived isotopic contaminants such as ^{60}Cu and ^{62}Cu.

We also demonstrated that 30 MeV α-accelerators, which are being developed for medical radionuclide production (e.g.,^{211}At), are viable for ^{61}Cu production. Under irradiation conditions of (30 MeV; 10 MeV energy loss; 3 h irradiation), the TTY^{EOB} reaches 420 MBq μA^{-1}, and after 1.8 h of cooling, the final yield is 290 MBq μA^{-1} with an RNP above 99.9%. Notably, this setup requires just one-third the target thickness used at 45 MeV, significantly reducing the amount of cobalt required.

Future work should focus on improving radiochemical separation techniques and further refining production strategies to meet clinical demand.

Moreover, the results obtained suggest that ^{59}Co(α,x) reactions, thanks to their favorable nuclear properties, wide range of product half-lives, and good agreement across experimental datasets are strong candidates for developing new monitor reactions for alpha particle beams, despite the higher cost of cobalt targets relative to standard materials such as aluminum or titanium.

CRediT authorship contribution statement

Irene Cardani: Writing – original draft, Investigation, Formal analysis, Data curation. **Michele Colucci:** Writing – review & editing, Writing – original draft, Validation, Supervision, Methodology, Investigation, Formal analysis, Data curation, Conceptualization. **Etienne Nigron:** Writing – review & editing, Visualization, Validation, Investigation. **Arnaud Guertin:** Writing – review & editing, Visualization, Validation, Supervision, Investigation. **Mariagabriella Marrella:** Writing – review & editing, Visualization, Investigation. **Ferid Haddad:** Writing – review & editing, Visualization, Validation, Supervision, Resources, Project administration, Funding acquisition. **Flavia Groppi:** Writing – review & editing, Visualization, Validation, Supervision, Resources, Project administration, Methodology, Investigation, Funding acquisition, Conceptualization. **Simone Manenti:** Writing – review & editing, Visualization, Validation, Supervision, Resources, Project administration, Methodology, Investigation, Funding acquisition, Conceptualization.

Declaration of competing interest

The authors declare that they have no known competing financial interests or personal relationships that could have appeared to influence the work reported in this paper.

Acknowledgments

This work has been funded by the CSN5 of the Italian National Institute of Nuclear Physics (INFN) through the project CUPRUM_TTD. The cyclotron Arronax is supported by CNRS, Inserm, INCa, the Nantes University, the Regional Council of Pays de la Loire, local authorities, the French government and the European Union. This work has been supported in part by the French National Research Agency (ANR) "France 2030 investment plan" under the references I-SITE NExT (ANR-16-IDEX-0007), and Labex DHOLMEN, by financial support from the Pays de la Loire Region and by a grant from INCa-DGOS-INSERM-ITMO Cancer_18011 (SIRIC ILIAD).

Data availability

Data will be made available on request.

References

Abbas, K., Kozempel, J., Bonardi, M., Groppi, F., Alfarano, A., Holzwarth, U., Simonelli, F., Hofman, H., Horstmann, W., Menapace, E., Lešetický, L., Gibson, N., 2006. Cyclotron production of^{64}Cu by deuteron irradiation of ^{64}Zn. Appl. Radiat. Isot. 64, 1001–1005.

Aliev, R.A., Moiseeva, A.N., Sergunova, K.A., Kormazeva, E.S., 2023. On the Use of Accelerated Helium Ions for Radionuclide Production: Are Beams of Alpha Particles Needed? Nanobiotechnology Rep. 18, 598–605. http://dx.doi.org/10.1134/S263516762360013X.

Ansari, M.A., Alslam, A., Mouner, A., Sathik, N.P.M., Ismail, M., Rashid, M.H., 2004. Excitation functions of α-induced reactions in cobalt and pre-equilibrium effects. Int. J. Mod. Phys. E 13, 585–595. http://dx.doi.org/10.1142/S0218301304002405.

Bashir, S., Shahzad, A., Bashir, S., 2019. Nuclear Medicine Physics. IntechOpen, London, England.

Basunia, M.S., 2018. Nuclear data sheets for A=59. Nucl. Data Sheets 151, 1–333. http://dx.doi.org/10.1016/j.nds.2018.08.001, https://www.sciencedirect.com/science/article/pii/S0090375218300590.

Bhat, M., 1998. Nuclear data sheets for A = 57. Nucl. Data Sheets 85, 415–536. http://dx.doi.org/10.1006/ndsh.1998.0021, https://www.sciencedirect.com/science/article/pii/S0090375298900217.

Biersack, J.P., Ziegler, J.F., 1982. The stopping and range of ions in solids. In: Ryssel, H., Glawischnig, H. (Eds.), Ion Implantation Techniques. Springer Berlin Heidelberg, Berlin, Heidelberg, pp. 122–156.

Bleuel, D., Bernstein, L., Marsh, R., Morrell, J., Rusnak, B., Voyles, A., 2021. Precision measurement of relative γ-ray intensities from the decay of^{61}Cu. Appl. Radiat. Isot. 170, 109625. http://dx.doi.org/10.1016/j.apradiso.2021.109625, https://www.sciencedirect.com/science/article/pii/S0969804321000385.

Boschi, A., Martini, P., Janevik-Ivanovska, E., Duatti, A., 2018. The emerging role of copper-64 radiopharmaceuticals as cancer theranostics. Drug Discov. Today 23, 1489–1501. http://dx.doi.org/10.1016/j.drudis.2018.04.002.

Browne, E., Tuli, J., 2013. Nuclear data sheets for A = 60. Nucl. Data Sheets 114, 1849–2022. http://dx.doi.org/10.1016/j.nds.2013.11.002, https://www.sciencedirect.com/science/article/pii/S0090375213000823.

Budzanowski, A., Grotowski, K., Kuzminski, J., Niewodniczanski, H., Strzalkowski, A., Sykutowski, S., Szmider, J., Wolski, R., 1967. Total reaction cross section and elastic scattering of 24.7 MeV alpha particles in the region of A = 60 nuclei. Nucl. Phys. Sect. A 106 (21), http://dx.doi.org/10.1016/0375-9474(67)90825-1.

Colucci, M., Bolchini, F.C., Confalonieri, L., Haddad, F., Nigron, E., Groppi, F., Manenti, S., 2024. Experimental cross-section measurement of the nuclear reactions induced by protons on ^{159}Tb: Evaluation of the ^{155}Dy/^{155}Tb precursor system. Radiat. Phys. Chem. 224, 112069.

Coura-Filho, G.B., Torres Silva de Oliveira, M., Morais de Campos, A.L., 2022. Nuclear Medicine in Endocrine Disorders : Diagnosis and Therapy. Springer International Publishing, Cham, Switzerland.

Das, S.S., Chattopadhyay, S., Barua, L., Das, M.K., 2012. Production of^{61}Cu using natural cobalt target and its separation using ascorbic acid and common anion exchange resin. Appl. Radiat. Isot. 70, 365–368. http://dx.doi.org/10.1016/j.apradiso.2011.10.011, https://www.sciencedirect.com/science/article/pii/S0969804311005264.

Gadioli, E., Gadioli Erba, E., Asher, J., Parker, D.J., 1984. Analysis of^{59}Co (α, x p y n z α) reactions up to 170 MeV incident α energy. Z. Phys. A 317, 155–168. http://dx.doi.org/10.1007/BF01421250.

Gilmore, G.R., 2008. Statistics of Counting. John Wiley & Sons, Ltd., pp. 101–129. http://dx.doi.org/10.1002/9780470861981.ch5, chapter 5.

Haddad, F., Ferrer, L., Guertin, A., Carlier, T., Michel, N., Barbet, J., Chatal, J., 2008. ARRONAX, a high-energy and high-intensity cyclotron for nuclear medicine. Eur. J. Nucl. Med. Mol. Imaging 35, 1377–1387.

Hermanne, A., Ignatyuk, A., Capote, R., Carlson, B., Engle, J., Kellett, M., Kibédi, T., Kim, G., Kondev, F., Hussain, M., Lebeda, O., Luca, A., Nagai, Y., Naik, H., Nichols, A., Nortier, F., Suryanarayana, S., Takács, S., Tárkányi, F., Verpelli, M., 2018. Reference cross sections for charged-particle monitor reactions. Nucl. Data Sheets 148, 338–382. http://dx.doi.org/10.1016/j.nds.2018.02.009, special Issue on Nuclear Reaction Data.

Hermanne, A., Tárkányi, F., Ignatyuk, A., Takács, S., Capote, R., 2023. Evaluated and recommended cross-section data for production of radionuclides with emerging interest in nuclear medicine imaging. Part 1: Positron emission tomography (PET). Nucl. Instruments Methods Phys. Res. Sect. B: Beam Interactions Mater. Atoms 535, 149–192. http://dx.doi.org/10.1016/j.nimb.2022.11.002, https://www.sciencedirect.com/science/article/pii/S0168583X22003238.

Hermanne, A., Tárkányi, F., Ignatyuk, A., Takács, S., Capote, R., 2025. Critical re-evaluation of recommended excitation functions of 7 reactions for ^{61}cu formation. Nucl. Instruments Methods Phys. Res. Sect. B: Beam Interactions Mater. Atoms 563, 165690. http://dx.doi.org/10.1016/j.nimb.2025.165690, https://www.sciencedirect.com/science/article/pii/S0168583X25000801.

Homma, Y., Murakami, Y., 1976. Production of ^{61}Cu by α- and^{3}He bombardments on cobalt target. Chem. Lett. 5, 397–400. http://dx.doi.org/10.1246/cl.1976.397.

Homma, Y., Murakami, Y., 1977. Production of ^{61}Cu by α and ^{3}He bombardment on cobalt target. Bull. Chem. Soc. Japan 50, 1251–1255. http://dx.doi.org/10.1246/bcsj.50.1251.

Huo, J., Huo, S., Yang, D., 2011. Nuclear data sheets for A = 56. Nucl. Data Sheets 112, 1513–1645. http://dx.doi.org/10.1016/j.nds.2011.04.004, https://www.sciencedirect.com/science/article/pii/S0090375211000457.

IAEA-NDS, 2025. Vchart — ensdf decay data visualization tool. https://www-nds.iaea.org/relnsd/vcharthtml/VChartHTML.html. (Accessed 01 June 2025).

Ismail, M., 1993. Measurement of excitation functions and mean projected recoil ranges of nuclei in α-induced reactions on F, Al, V, Co and Re nuclei. 40, pp. 227–251. http://dx.doi.org/10.1007/BF02900190.

Ismail, M., Divatia, A.S., 1988. Measurement and analysis of alpha-induced reactions on Ta, Ag and Co. 30, pp. 193–210. http://dx.doi.org/10.1007/BF02846693.

Jastrzębski, J., Singh, P.P., Mróz, T., Vigdor, S.E., Fatyga, M., Karwowski, H.J., 1986. Interaction of 5-50 MeV/nucleon ^{3}He and ^{4}He with ^{59}Co. Phys. Rev. C 34, 60–79. http://dx.doi.org/10.1103/PhysRevC.34.60.

Keinñen, O., Brennan, J.M., Membreno, R., Fung, K., Gangangari, K., Dayts, E.J., Williams, C.J., Zeglis, B.M., 2019. Dual radionuclide theranostic pretargeting. Mol. Pharm. 16, 4416–4421.

Koning, Arjan, Hilaire, Stephane, 2023. TALYS: modeling of nuclear reactions. Eur. Phys. J. A 59, 131. http://dx.doi.org/10.1140/epja/s10050-023-01034-3.

Levkovskij, V.N., 1991. Activation cross sections for the nuclides of Medium Mass Region (A = 40–100) with medium energy (E = 10–50 MeV) protons and alpha-particles.

Loveland, W., Morrissey, D., Seaborg, G., 2006. Modern Nuclear Chemistry. John Wiley & Sons.

Michel, R., Brinkmann, G., 1980. Alpha-induced reactions on cobalt. Nucl. Phys. A 338, 167–189. http://dx.doi.org/10.1016/0375-9474(80)90128-1.

Mou, L., Martini, P., Pupillo, G., Cieszykowska, I., Cutler, C.S., Mikołajczak, R., 2022.^{67}Cu production capabilities: A mini review. Molecules 27, http://dx.doi.org/10.3390/molecules27051501.

Mukherjee, S., Sharma, A.K., Bakhru, D., Singh, N.L., Kolev, D., 1998. Pre-equilibrium alpha and nucleon emission in^{59}Co (α, zαypxn) reactions. Phys. Scr. 58, 319. http://dx.doi.org/10.1088/0031-8949/58/4/007.

Müller, C., Domnanich, K.A., Umbricht, C.A., van der Meulen, N.P., 2018. Scandium and terbium radionuclides for radiotheranostics: current state of development towards clinical application. Br. J. Radiol. 91, 20180074–20180074.

Neuzil, E.F., Lindsay, R.H., 1963. Emission of Be^{7} and competition processes at 30 to 42 MeV. Phys. Rev. 131, 1697–1701. http://dx.doi.org/10.1103/PhysRev.131.1697.

Otuka, N., Takács, S., 2015. Definitions of radioisotope thick target yields. Radiochim. Acta 103, 1–6.

Pupillo, G., Mou, L., Manenti, S., Groppi, F., Esposito, J., Haddad, F., 2022. Nuclear data for light charged particle induced production of emerging medical radionuclides. Radiochim. Acta 110, 689–706. http://dx.doi.org/10.1515/ract-2022-0011.

Qaim, S.M., 2020. Medical Radionuclide Production. De Gruyter.

Qaim, S.M., 2024. New directions in nuclear data research for accelerator-based production of medical radionuclides. J. Radioanal. Nucl. Chem..

Rama Rao, J.., Mohan Rao, A., Mukherjee, S., Upadhyay, R., Singh, N., Agarwal, S., Chaturvedi, L., Singh, P., 1987. Excitation functions of alpha particle induced reactions in cobalt in the energy range 10–120 MeV using variable energy cyclotrons. Nucl. Instruments Methods Phys. Res. Sect. B: Beam Interactions Mater. Atoms 24-25, 484–489. http://dx.doi.org/10.1016/0168-583X(87)90689-6.

Sadeghi, M., Amiri, M., Roshanfarzad, P., Avila, M., Tenreiro, C., 2008. Radiochemical studies relevant to the no-carrier-added production of$^{61,\ 64}$Cu at a cyclotron. Radiochim. Acta 96, 399–402. http://dx.doi.org/10.1524/ract.2008.1504.

Singh, N.L., Agarwal, S., Rao, J.R., 1993. Excitation function for α-particle-induced reactions in light-mass nuclei. Can. J. Phys. 71, 115–121. http://dx.doi.org/10.1139/p93-017.

Skulski, W., Fornal, B., Broda, R., Jastrzebski, J., Koczoń, P., Kownacki, J., Opacka, M., Pawłat, T., Pieńkowski, L., Płóciennik, W., Sieniawski, J., Singh, P.P., Styczeń, J., Wrzesiński, J., 1992. Mass and charge release by the evaporation of particles from compound nuclei around mass 60. Z. Phys. A - Hadron. Nucl. 342, 61–66. http://dx.doi.org/10.1007/BF01294489.

Stearns, C.M., 1962. Comparison of Reactions of Copper-63 Compound Nuclei Performed By Alpha-Particle, Proton, and Carbon-Ion Bombardments (thesis). Faculty of Pure Science, Colombia University.

Szelecsényi, F., Steyn, G., Kovács, Z., van der Walt, T., Suzuki, K., 2006. Comments on the feasibility of^{61}Cu production by proton irradiation of (nat)Zn on a medical cyclotron. Appl. Radiat. Isot. 64, 789–791.

Szelecsényi, F., Suzuki, K., Kovács, Z., Takei, M., Okada, K., 2002. Production possibility of $^{6}0,6162$Cu radioisotopes by alpha induced reactions on cobalt for PET studies. Nucl. Instruments Methods Phys. Res. Sect. B: Beam Interactions Mater. Atoms 187, 153–163. http://dx.doi.org/10.1016/S0168-583X(01)00923-5.

Tárkányi, F., Hermanne, A., Ignatyuk, A.V., Ditrói, F., Takács, S., Capote-Noy, R., 2024. Extension of evaluated cross section database for charged particle monitor reactions. J. Radioanal. Nucl. Chem. 333, 4243–4331. http://dx.doi.org/10.1007/s10967-024-09513-7.

Verpelli, M., Abriola, D., 2011. Information management tools for evaluated nuclear structure data file (ensdf) interrogation and dissemination. J. Korean Phys. Soc. 59, 1322–1324. http://dx.doi.org/10.3938/jkps.59.1322.

Yang, D., Huo, J., 2014. Nuclear data sheets for A = 54. Nucl. Data Sheets 121, 1–142. http://dx.doi.org/10.1016/j.nds.2014.09.001, https://www.sciencedirect.com/science/article/pii/S0090375214006553.

Zhukova, O.A., Kanashevich, V.I., Laptev, S.V., Chursin, G.P., 1972. Nuclear reactions produced by alpha particles on^{59}Co nuclei. Yad. Fiz. 16, 242, English translation: Sov. J. Nucl. Phys. 16 (1973) 134.

Zuber, K., Singh, B., 2015. Nuclear data sheets for A = 61. Nucl. Data Sheets 125, 1–200. http://dx.doi.org/10.1016/j.nds.2015.02.001, https://www.sciencedirect.com/science/article/pii/S0090375215000022.